

Impacts and Proficiency of Merging the Photovoltaic and Wireless Charging System for Electrical Transportation Sector

Asma BOUKHCHANA, Mohamed NAOUI, Aymen FLAH, Habib KRAIEM*

Abstract: Using dynamic wireless charging systems in conjunction with electric vehicles (EV) could revolutionize transportation in the future by enabling faster driving and non-stop battery charging. Dynamic wireless power transfer can fix the autonomy problems with electric vehicles. The fact that this charging device gets its power from the electrical grid has some serious drawbacks, too. Utilizing alternate sources, like PV generators, is therefore seen to be a potential answer. This study aims to illustrate the advantages that can arise from the interplay of renewable energy sources with wireless recharge systems for electric vehicles in this environment. Therefore, this paper is built and has regrouped the needed sections that can define the wireless recharge concept based on an alternative energy source. Simulation results were adapted by the Matlab Simulink platform, where more than one situation is tested and examined. This is by testing the influence of the vehicle's speed on the wireless charging performances and by testing what effect can be done if the climatic conditions are varied, especially on the global performances of the wireless recharge tool.

Keywords: battery state of charge; coils; competences; electric vehicles; on road charge; wireless charging

1 INTRODUCTION

Electric vehicles (EV) are currently growing rapidly as a result of five important trends around the world: the depletion of fossil fuels and the associated rise in fuel prices; the public's growing knowledge of and desire to tackle climate change; the development of new commercial effectiveness of technology for renewable energy; the advancement of electric motors and electronic control systems that directly manage EV propulsion; improvements in EV enabling technologies like Vehicle-to-Grid (V2G) and Grid-to-Vehicle (G2V) [1].

Fossil fuels are under pressure globally; thus, many nations are turning to dependable, affordable, efficient, and environmentally friendly energy sources. As one of the largest sources of CO₂ emissions, fossil fuels pose a serious threat to the environment. Fig. 1 depicts the percentage contribution of CO₂ emissions by the electricity and heat sector, the transportation sector, the industrial sector, the housing sector, and other regions, claims the International Energy Agency [2].

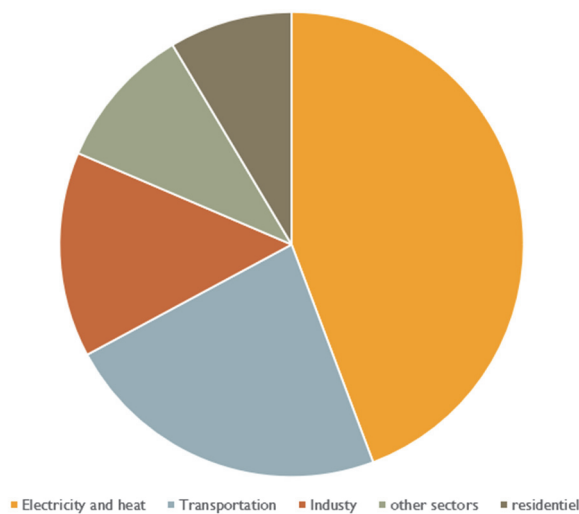


Figure 1 CO₂ emissions by different sectors

In 2020, transport is considered one of the most important sectors that contributes 22% of gas emissions.

Most public and private vehicles use internal combustion engines (ICE), which are one of the primary contributors to climate change. On the other hand, electric vehicles do not directly emit CO₂ or are less susceptible to high oil prices [3].

Much work has been done globally to integrate environmentally friendly energy sources like solar and wind power. The transition from petrol-fueled mobility to electric mobility is the current trend in transportation. The two tendencies could be combined to create an electric mobility system that uses green energy [4].

The two main disadvantages of electric vehicles over conventional vehicles are their short driving range and high price, both resulting from current battery technology and specifications. Increasing driving range and/or reducing battery size is possible with the widespread use of on-road charging facilities. Therefore, such systems offer a solution to overcome the existing electric mobility limitations.

Charging systems are the primary factor influencing the growth of EV. Static charging is frequently regarded as a viable temporary measure to counter low-voltage grid congestion from EV charging, thereby circumventing hefty grid upgrade expenses. Studies [5-8], the efficacy of static charging schedules for EVs is highlighted as a short-term remedy for grid congestion. These researches juxtapose static and dynamic charging techniques, delving into the advantages and drawbacks of each. On the other hand, as elaborated in [7], dynamic charging enables EVs to recharge on the move [9, 10], fostering power interaction between the vehicle and the grid without the need for stationary charging infrastructures. This method boasts numerous benefits, such as enhanced energy transfer efficiency, negligible vehicle downtime during charging, and a diminished environmental footprint as noted in [11]. Given these advantages, our research predominantly leans towards the dynamic charging strategy.

In this work we are interested in wireless dynamic charging technology. This technology offers faster driving without having to stop to recharge in conjunction with electric vehicles and automated and connected vehicles [12-14]. Inductive coupling is one of the most often used techniques for dynamic wireless charging systems to supply energy from the transmitting coils located on the

ground of the road to the receiving coils located under electric vehicles. According to Fig. 2, the transmitters and receivers build a loosely coupled transformer that delivers power by mutual inductance across an air gap.

This study used photovoltaic panels to power the wireless dynamic charging system. These generate the DC current. They are connected by a converter boost to increase the supply voltage from that of the load. This converter is connected to the inverter, which converts the DC current into AC current to power the coil issuer [15]. This creates a magnetic field, which converts magnetic energy into energy to power the take-up reel. This coil is linked to the rectifier which converts AC current into DC current to charge the electric vehicle's battery [16].

The authors of studies [17] and [18] delved into different coil designs for wireless power transfer in electric vehicle battery charging. A comparative analysis of various coil shapes was presented in [18]. Utilizing Ansys for modeling, they assessed the performance of both circular and rectangular coils. The findings underscored the superiority of the rectangular coil over the circular design and other shapes. As a result, our research predominantly concentrates on the design of rectangular coils.

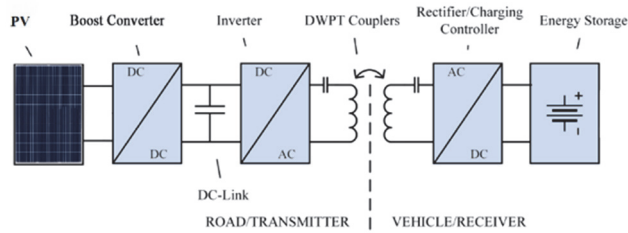


Figure 2 An electric vehicle wireless charger's structural design

Public and private recharging infrastructures must be deployed with adequate coverage to provide the necessary thrust for EV arrival. These recharging infrastructures may be supplied by the electrical grid or by renewable energy sources. The modalities of recharge (fast or gradual) may differ during the use of these various energy sources, necessitating the sizing of recharge systems and the modification of installations. The propulsion systems for electric vehicles often include a few components that work together to maintain the vehicle's high power and road stability. The charging mechanism is coupled to most of these components. In this approach, the power transfer without a dynamic link is a useful technique for handling electrical vehicle issues. On the other hand, there is a significant drawback to this recharge system's connection to the electrical network's energy source.

In studies [5, 19], the authors utilized the electric grid to power electric vehicle charging systems. Often, these grids rely on fossil fuels for electricity generation, which negatively impacts the environment. To address this concern, our approach shifts away from grid energy, emphasizing the use of solar energy for EV charging [20, 21].

With pure electric vehicles, wireless charging has long been popular. It is made to make it possible to recharge the battery while the vehicle is moving. This method's complex working philosophy, which involves the existence of several variables and parameters, makes it difficult to

examine. In addition, a variety of other criteria, like the vehicle's speed and the widths and lengths of its receptacles, depend on the condition of the vehicle - whether it is moving or not. It provides a fresh way to improve the dynamic wireless charging system's efficiency.

The fundamental idea of this work is to describe the various variables that can react to the performances of the wireless recharge system, and the paper's purpose is elaborated based on these study findings. This was studied by testing different architectures and concepts that can be used for charging the vehicle in wireless mode. Even though previous results have demonstrated that the wireless recharge technology can be profitable, some weaknesses have appeared if the highway roads are in question for making this technology for users. The major problem is the requirement for electrical power to supply the recharge system. On highway roads, this is not always available. This is why this paper has exposed PV systems as an alternative and sustainable energy source. Studying this complex system is the main objective of this paper. So as supposed outcomes of this work are to verify the ability of integration of renewable energy for enhancing the electric vehicle recharge even if the vehicle is on road. The parameters that influence the global performances must be depicted and tested. Evaluating the performances of the wireless recharge tool for various vehicle speeds and looking for the best combination of this recharge system seem to be the global outcomes of this research work.

2 EVS WIRELESS CHARGER OPERATION

2.1 The Wireless Recharge Concept

This study examines wireless power transfer technology, which has two main components: one for the road and another for the car. The part of the road that is permanently fixed is the transmitter. The second part, situated below the car, is the moving receiver. Each component has an electronic system, and an air gap separates them. The transmitter block generates a high frequency, alternating magnetic flux. This magnetic flux, which the receiver coil connects to and then transforms into electric energy, is utilized to refuel the electric vehicle's battery. Two electric vehicle (EV) examples with wireless charging stations are shown in Fig. 3. They are both parked on a road. One only has one receiver, whereas the other has two [22].

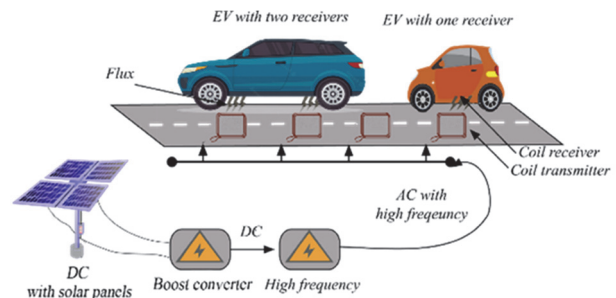


Figure 3 Composition of the wireless charging system

The functional layout of the electric vehicle's wireless charger is shown in Fig. 1. The input DC voltage source, or V_{in} , is defined by the Society of Automotive Engineers

(SAE) J2954 standard as having a typical range of 350 to 500 V_{DC} . The primary inductance (L_p) displays the self-inductance of the transmitter coil, the secondary inductance (L_s) displays the self-inductance of the receiver coil, and M represents the mutual inductance between the transmitter and the receiver. A boost converter normally generates the input voltage V_{in} , and an inverter transforms the input voltage (V_{in}) into an alternative voltage with high frequency that is fed to the primary compensation tank, which consists of capacitive and inductive resonances. The primary resonant tank serves as a limited filter, allowing fundamental-frequency signals to pass while blocking elevated frequencies, and compensates for the reactive power of the magnetic coupler's significant coupled inductor. Therefore, AC voltage is used to power the primary coil. The wireless charging system's output power is inversely proportional to the transmitter current [23]. The transmitter current is commonly kept constant to simplify the output power control technique. The secondary side of the system receives a second resonant tank to increase system efficiency and power transmission capacity. Also, it eliminates the magnetic coupler unit's substantial leakage inductance. After passing through the resonant tank, an inverter solves the induced voltage at the reception coil. In contrast to the conductive charger, the primary side of the wireless charger is positioned on the vehicle while the secondary side is located off-board.

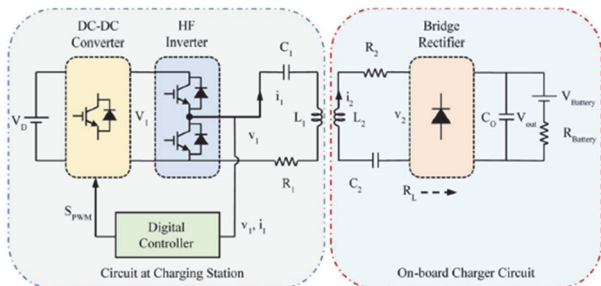


Figure 4 Diagram block of the onboard EV charger with the developed controller

2.2 Topologies for Compensation

The connection between the primary and secondary sides is poor due to the large separation. As a result, given the high reactive power, the employment of resonance elements on both sides is required as compensation to maintain optimal efficiency and to accomplish the desired amount of transferred power. It is also necessary to modify the output parameters on the load side to guarantee that the charger functions at a particular voltage with the current the battery needs.

The inductive energy transfer system might be used with either of the four resonant circuit topologies. They are called parallel (P) or series (S) connections depending on where the capacitor resonance is inserted on each side. Tab. 1 shows the representation of different strategies of compensation: SS , SP , PS , and PP [24, 25].

Inductances (L_p , L_s) and (C_1 , C_2) are selected to cancel the reactive portion of the transferred power. Reduce the apparent power from the source of entry and ensure that the active power is transmitted to the load to improve power transfer [26, 27].

Each circuit's voltage gain (G_v) is defined as the proportion of the input voltage (V_{in}) to the output voltage (V_o). It is crucial to recognize the crucial variables of input impedance, efficiency, and output voltage gain

$$\left(G_v = \frac{V_o}{V_{in}} \right)$$

to analyze any resonant architecture. The input impedance can be used to calculate the input phase angle, input current, and voltage gain as a function of the resonant elements. With a misalignment-tolerant design, the efficiency and voltage gain are expected to be less dependent on the coupling factor. The schematics, output voltage gains, and input impedances of the most widely used topologies are reviewed in Fig. 5.

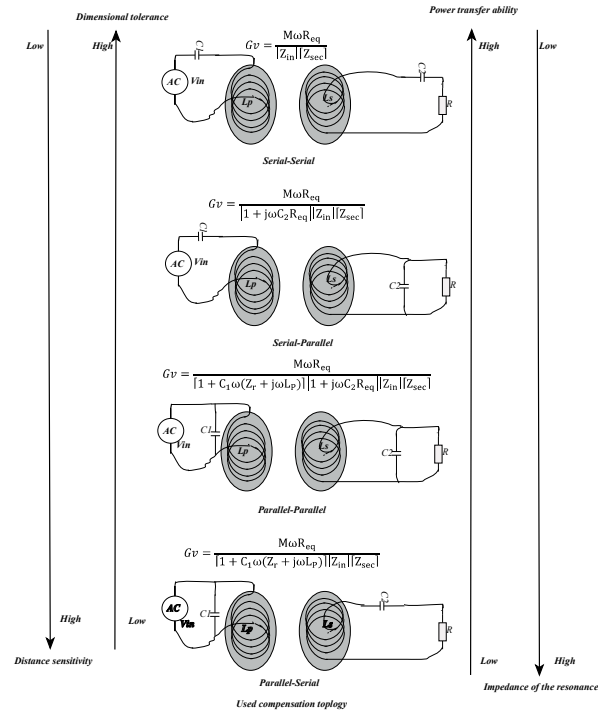


Figure 5 Wireless charging features [28, 29]

Table 1 Several typical resonant topologies are defined by voltage gain and impedance

Topology	Impedances
SS	$Z_{in} = \frac{1}{j\omega C_1} + j\omega L_p + Z_r$ $Z_{sec} = j\omega L_s + \frac{1}{j\omega C_2} + R_{eq}$
SP	$Z_{in} = \frac{1}{j\omega C_1} + j\omega L_p + Z_r$ $Z_{sec} = \left(R_{eq}^{-1} + j\omega L_s^{-1} + j\omega C_2^{-1} \right)^{-1}$
PP	$Z_{in} = \left(j\omega C_1 + \frac{1}{j\omega L_p + Z_r} \right)^{-1}$ $Z_{sec} = \left(R_{eq}^{-1} + j\omega L_s^{-1} + j\omega C_2^{-1} \right)^{-1}$
PS	$Z_{in} = \left(j\omega C_1 + \frac{1}{j\omega L_p + Z_r} \right)^{-1}$ $Z_{sec} = j\omega L_s + \frac{1}{j\omega C_2} + R_{eq}$

2.3 The Concept of Wireless Charging's Mathematical Model

There are two types of charging: static charging, which several companies use and continue to develop. We use the Waseda Electric Bus in Japan as an example, which has a power range of 30 to 150 kW and 105 mm between the transmitter and receiver coils. While using this approach, the car charges every time it passes by a bus stop [30].

Dynamic charging is the second kind of charging. Under this charging method, the vehicle charges while in motion. This is accomplished using a specially designed track with coils that only become active when a passing vehicle passes. With this approach, it may be possible to lower the vehicle's battery capacity and, as a result, its weight and cost.

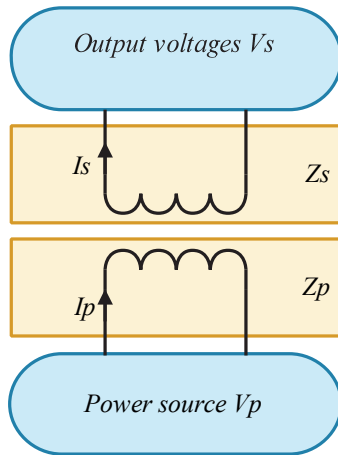


Figure 6 The system for wireless charging is illustrated simply

Fig. 6 shows a simplified representation of this wireless charging technology. The input and output voltages of this technology are denoted V_p and V_s as shown in Eqs. (6) and (7) [31]. Eq. (1) can represent the model of mutual inductance coupling because it is connected to the impedance formulation [32].

with:

$$\begin{cases} Z_{(p,s)} = kj\omega MI_s \\ k = -1 & \text{if } Z_p \\ k = 1 & \text{if } Z_s \end{cases} \quad (1)$$

where: M - Mutual inductance; ω - angular frequency; I_s - The secondary current.

The magnetic coupling coefficient is related to the mutual inductance by this equation:

$$C_k = \frac{M}{\sqrt{L_p L_s}} \quad (2)$$

Z_r is used in this equation to represent the reflected impedance from the secondary to the primary:

$$Z_r = \frac{\omega^2 M^2}{Z_s} \quad (3)$$

By using the selected compensation topology, Z_s is the secondary impedance, and the following equation provides the current flowing through the secondary winding:

$$I_s = \frac{j\omega MI_p}{Z_s} \quad (4)$$

This equation indicates that the primary and secondary resonant frequencies are the same:

$$\omega = \frac{1}{\sqrt{C_{(p,s)} L_{(p,s)}}} = 2\pi f \quad (5)$$

or:

$C_{(p,s)}$: Primary and secondary capacitor.

$L_{(p,s)}$: Primary and secondary inductance.

The primary voltage can be written as follows:

$$V_p = j2\pi f_r L_p I_p - j2\pi f_r M I_s \quad (6)$$

This relationship expresses the secondary voltage:

$$V_s = j2\pi f_r M I_p - j2\pi f_r L_s I_s \quad (7)$$

The primary power equation is:

$$P_p = V_p I_p \quad (8)$$

The secondary power is given in Eq. (9):

$$P_s = V_s I_s \quad (9)$$

The primary coil's proportional flux is expressed in Eq. (10) as a function of related physical variables. This equation assumes that the centers of two coils are matched to allow proper transmission of magnetic flux. The flux Φ_s obtained in the secondary coil "attached to the vehicle" in the mobility example, however, is described as the goal of the first flux established if the two coils are jumbled.

$$\begin{cases} \Phi_p(t) = \left(\frac{\mu_0 \cdot S \cdot N^2}{l} \right) I_p(t) \\ \Phi_s = \varepsilon \cdot \Phi_p \end{cases} \quad (10)$$

where: N - Number of turns; l - Length of the solenoid; I_p - Primary current; S - Surface; B - The magnetic field; μ_0 - The magnetic constant.

The new dynamic model method of the wireless charging system is based on the parameter ε .

The following Tab. 2 presents the relation between the parameter ε , the length l_{t-r} between the transmitter coil and the receiver coil, the length l_c that defines the offset between the centers of two coils, and the length of the transmitter coil l_t .

Table 2 The relationship between the parameter ε and the lengths that define the magnetic field

Parameter ε	dimensions l_{c-r} , l_c and l_t
$\varepsilon=0$	$l_c > l_t$
$\varepsilon=1$	$l_c = 0$
$0 < \varepsilon < 1$	$0 < l_c < l_t$

The inductance factor "L" is related to the shape of the coil, in this case the shape is flat rectangular. Therefore, "L" can be expressed as follows:

$$L = K_1 B_0 \frac{N d_m}{1 + K_2 \rho} \tag{11}$$

K_1 and K_2 denote the empirical coefficients ($K_1 = 2,34$ and $K_2 = 2,75$), B_0 presents Vacuum permeability ($B_0 = 4\pi \cdot 10^{-7}$ H/m), d_m is the average diameter, and ρ presents the rate at which the coil is being filled.

With

$$\rho = \frac{d_{out} - d_{in}}{d_{out} + d_{in}} \tag{12}$$

The filling rate ρ reflects how hollow the spiral is. In the case of a small model ρ , the coil is hollow ($d_{out} \approx d_{in}$) and in the case of a large model ρ , the coil is full ($d_{out} \gg d_{in}$).

The following figure shows the winding characteristics.

$$\rho = \frac{d_{out} - d_{in}}{d_{out} + d_{in}}$$

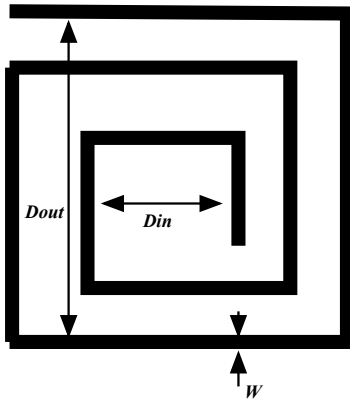


Figure 7 Winding characteristics

2.4 The Associated Converters with the Wireless Recharge System

The primary objective of this study, as stated in the paper's objective, is to present a solution for feeding the wireless transmitter which exists on a long road by the necessary power. The appropriate DC/DC converter will be installed first to make the relationship with the PV panels. Then, the DC/AC inverter will be installed to manage the needed frequency signal for the first transmitter. Fig. (8), gives the appropriate converter designs and relationships [33, 34].

The boost converter is typically used in converting a low input voltage to an output voltage. It has an input voltage V_i source DC, an inductance L , a switch K , a diode D , and two capacitors C_1 and C_2 . Fig. 8 designs the equivalent electrical diagram of the boost converter.

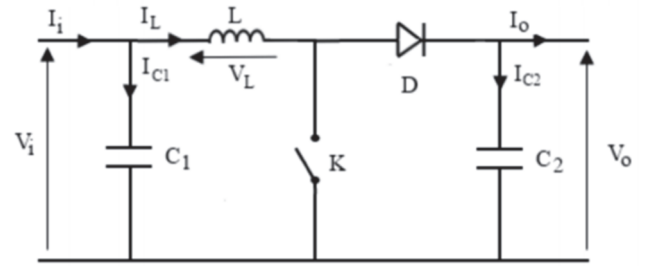


Figure 8 Converter DC/DC

The corresponding duty cycle is expressed as follows:

$$\frac{V_o}{V_i} = \frac{1}{1 - D} \tag{13}$$

Eqs. (14) and (15) give the expression for capacitance and inductance respectively of the needed filter [35] :

$$C = \frac{D V_o}{f_s R \Delta V} \tag{14}$$

$$L = \frac{D V_i}{f_s \Delta I} \tag{15}$$

The corresponding equation depends on the switch K position, so:

If the switch K is open, the equations can be expressed as follows:

$$\begin{cases} I_{c1} = C_1 \frac{dV_i}{dt} = I_i - I_L \\ I_{c2} = C_2 \frac{dV_o}{dt} = I_L - I_o \\ V_L = L \frac{dI_L}{dt} = V_i - V_o \end{cases} \tag{16}$$

However, if the switch K is closed, the equations can be written in the form of the Eq. (17):

$$\begin{cases} I_{c1} = C_1 \frac{dV_i}{dt} = I_i - I_L \\ I_{c2} = C_2 \frac{dV_o}{dt} = -I_o \\ V_L = L \frac{dI_L}{dt} = V_i \end{cases} \tag{17}$$

The second converter part is the inverter that provides a single-phase alternating voltage at its output. To assemble the power circuit of the inverter. Fig. 9 shows the inverter wiring diagram (DC/AC converter).

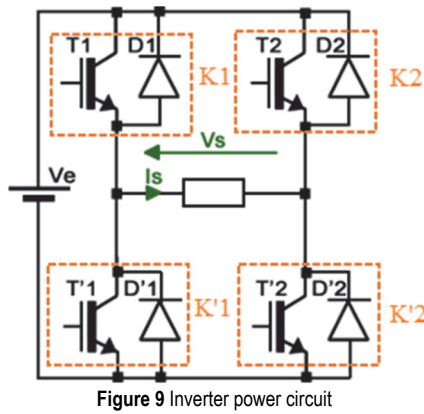


Figure 9 Inverter power circuit

The states of the switches can be determined by the value at the terminals of the load type as an inductive case:

For $0 \leq t \leq \frac{T}{2}$: K1 and K'2 are ON while K2 and K'1 are OFF, therefore the output voltage is expressed as in Eq. (18).

$$V_s = L \frac{di}{dt} + Ri = V_e \tag{18}$$

The current expression can be written as follows:

$$i(t) = \frac{V_e}{R} \left(1 - e^{-\frac{t}{\tau}} \right) - I_M e^{-\frac{t}{\tau}} \tag{19}$$

For $\frac{T}{2} \leq t \leq T$: K2 and K'1 are ON while K1 and K'2 are OFF, the output voltage will be as in Eq. (20).

$$V_s = L \frac{di}{dt} + Ri = -V_e \tag{20}$$

Finally, we find this expression of the current:

$$i(t) = \frac{V_e}{R} \left(1 - e^{-\left(\frac{t - \frac{T}{2}}{\tau} \right)} \right) + I_M e^{-\left(\frac{t - \frac{T}{2}}{\tau} \right)} \tag{21}$$

2.5 The Power Storage System

This item is modelled to show the efficiency of the wireless charging tool and the energy flow analyzer. The main battery design is shown in Fig. 10.

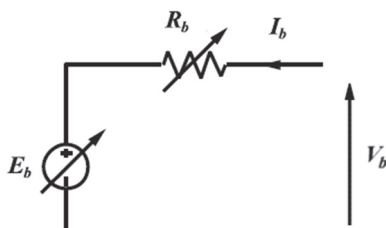


Figure 10 Battery lithium-ion circuit

This has a DC voltage source and a variable resistor in series which depends on many parameters as shown in Eq. (22), where the charge/discharge voltage of the lithium-ion battery is described [27].

$$V_b = \begin{cases} V_{b\text{-charge}} = E_b + R_b I_b \\ V_{b\text{-discharge}} = E_b - R_b I_b \end{cases} \tag{22}$$

The battery's residual capacity $Q(t)$ is defined as it is in Eq. (23):

$$Q(t) = Q(0) \int_0^t (\eta_b I_b) dt \tag{23}$$

where: η_b - Battery performance; t - Discharge time, I_b - Battery current.

The state of charge SOC can be expressed as:

$$SOC\% = \left(\frac{Q(t)}{Q_{max}} \right) 100 \tag{24}$$

where: Q_{max} - The maximum capacity.

The battery voltage charge and discharge (E_b) is specified by the internal elements of the battery and is expressed as:

$$E_b = \begin{cases} E_0 - K_b \left(\frac{Q}{Q-it} \right) i^* - K_b \left(\frac{Q}{Q-it} \right) it + Ae^{(-B.it)} \\ \rightarrow \text{discharge } i^* > 0 \\ E_0 - K_b \left(\frac{Q}{0.1Q+it} \right) i^* - K_b \left(\frac{Q}{Q-it} \right) it + Ae^{(-B.it)} \\ \rightarrow \text{charge } i^* < 0 \end{cases} \tag{25}$$

where: E_0 is the Battery constant voltage; K_b is the polarization resistance; i^* is the filtered battery current,

It is the extracted capacity; A is the voltage corresponding to the end of the exponential zone; B is the capacitance corresponding to the exponential zone.

3 SOURCE OF POWER DESCRIPTION: PV GENERATOR

As it has been exposed before, solar energy will be managed to be the main energy source for this recharge system. So, firstly a description of the solar PV will be done. Then, we try to describe an overall PV panel model. A PV module is formed of several PV cells connected in series and parallel to produce the necessary voltage and current levels.

The general model's equivalent circuit is composed of a photo current (I_{ph}), a diode current, a parallel resistance (R_{sh}) that expresses a leakage current, and a series resistance (R_s) brought on by the contacts between semiconductors and metallic parts [36, 37].

We employ Kirchoff's law in Fig. 11. The following equation will get the current:

$$I_c = I_{ph} - I_D - I_{sh} \quad (26)$$

where I_{ph} is the photo current produced by light and I_{sh} is the parallel resistor current, which can be calculated as:

$$I_{sh} = \frac{V_c + R_s I_c}{R_{sh}} \quad (27)$$

The saturation current is proportional to the diode current I_D . The following equation gives the value of this magnitude:

$$I_D = I_{sd} \times \left[\exp\left(\frac{q \cdot (V_c + R_s I_c)}{n \cdot K \cdot T}\right) - 1 \right] \quad (28)$$

where: I_{sd} - The reverse saturation current; q - The electron charge ($1.6 \times 10^{-19} C$); K - The Boltzmann constant ($1.38 \times 10^{-23} J/K$); T - The cell temperature measured in Kelvin (K); n - The ideal factor.

We substitute the characteristic current-voltage equation of a solar cell in Eq. (26). So, we conclude:

$$I_c = I_{ph} - I_{sd} \times \left[\exp\left(\frac{q \cdot (V_c + R_s I_c)}{n \cdot K \cdot T}\right) - 1 \right] - \frac{V_c + R_s I_c}{R_{sh}} \quad (29)$$

The resistance R_s and the resistance R_{sh} influence the characteristic $I = f(V)$ of the PV cell:

The serial resistance (R_s) is the cell's internal resistance depending mainly on the semiconductor's resistance, the contact resistance of the collector grids and the sensitivity of the shunt resistance (R_{sh}) is due to a leakage current at the junction; it depends on how it was made.

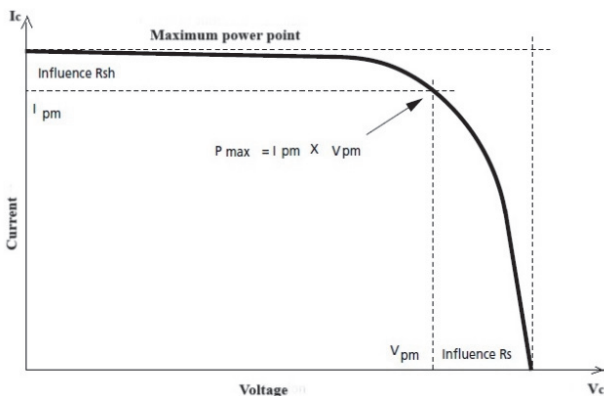


Figure 11 Influence of serial and shunt resistors on the current-voltage characteristic of a PV cell

According to the equation below, solar radiation and cell operating temperature have a major role in determining the photocurrent:

$$I_{ph} = \left[I_{sc} + K_i (T - T_{ref}) \right] \frac{G}{G_{ref}} \quad (30)$$

The overall structure of the PV generator is given in the following Fig. 12:

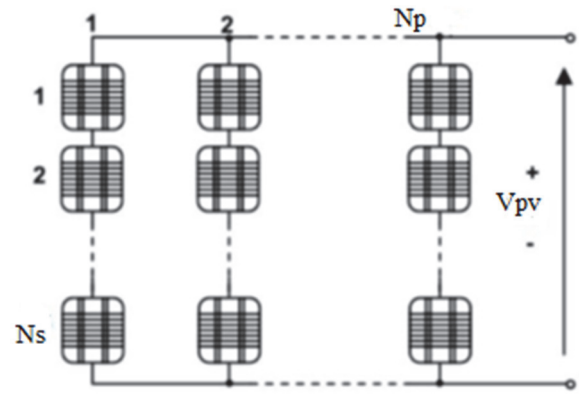


Figure 12 Photovoltaic generator

Considering the same brightness and temperature over the entire panel, the generated current can be described as follows [38].

$$I_{PV} = N_p I_{ph} - N_p I_{sd} \cdot \left[e^{\frac{q \left(\frac{V_c + R_s I_c}{N_s + N_p} \right)}{n \cdot K \cdot T}} - 1 \right] - \left(\frac{N_p V_c + R_s I_c}{R_{sh}} \right) \quad (31)$$

4 WIRELESS CHARGING SYSTEM DESIGN FOR A HIGHWAY APPLICATION

The 3D model of the transmitter and receiver coils was made using ANSYS Maxwell. The distance between the two copper coils is 20 cm. A rectangular transparent plate was positioned between the two coils to record the magnetic field that had been produced between them. The simulations would be carried out in an area measuring (120 cm, 240 cm, and 120 cm). The solution designed through the ANSYS Maxwell software is to establish a boundary for the location of the two coils. The design of the transmitter and receiver coils is shown in Fig. 13. The corresponding parameters of the coils and plate in the simulation phase are summarized in Tabs. 3 and 4, respectively.

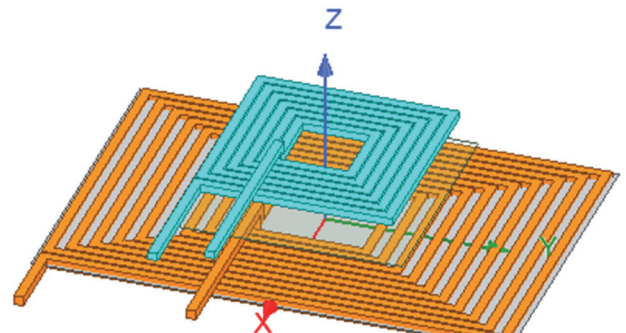


Figure 13 The 3D model of the transmitter and receiver coils

Table 3 Coil characteristics

Parameter	Variable	Value
Primary coil length in the X -direction	L_{px}	80 cm
Primary coil length in the Y -direction	L_{py}	120 cm
Primary coil width	W_p	2.5 cm
The primary side's turn number	N_p	10
Air gap	G	20 cm
Secondary coil length in the X -direction	L_{sx}	50 cm
Secondary coil length in the Y -direction	L_{sy}	50 cm
Secondary coil width	W_s	2.5 cm
The secondary side's turn number	N_s	6
Reference		[39]

Table 4 Rectangular plate components

Name	Value	Unit
Position	-30, -30, 10	cm
Axis	Z	
X Size	60	cm
Y Size	60	cm

In ANSYS Maxwell, Fig. 14 shows the transmitter and receiver coils and their magnetic fields. The magnetic field between the coils decreases when the distance between them increases. We have discovered that the coupling coefficient between the two coils increases as the distance between them decreases.

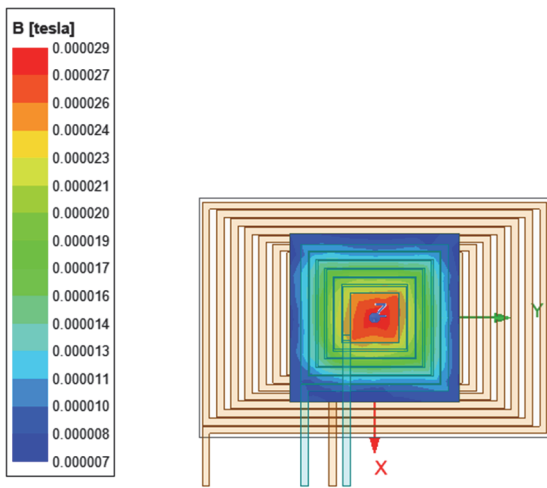


Figure 14 The magnetic field between the transmitter and receiver coils

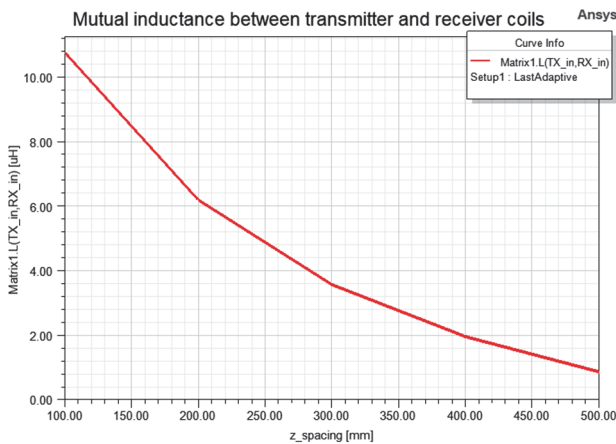


Figure 15 Mutual inductance between transmitter and receiver coils

The amount of mutual inductance between the coils changes slightly, as shown in Fig. 15, because each coil

corresponds to the sum of its inductance and the mutual inductance of the other coil. The definition of the excitation current track causes a small change in rate when the other coil approaches since there is still some flux.

ANSYS Electronics software was used to create the overall schematic for the wireless charging system.

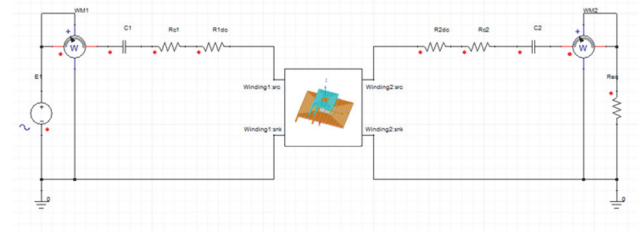


Figure 16 Wireless charging system on ANSYS Maxwell

Fig. 16 shows the wireless charging setup with SS topology. In the primary part, on an energy source of frequency 150 kHz and voltage 280 V. In the middle, on the two transmitter and receiver coils, the corresponding capacitors and resistor values are summarized in Tab. 5.

To calculate the different characteristics, there are two wattmeters.

Table 5 The value of the components of the electrical circuit

Components	Value
Capacitor C_1	27.16 nF
Resistance R_{C1}	14.38 M Ω
Resistance R_{1dc}	12.2 M Ω
Capacitor C_2	27.16 nF
Resistance R_{C2}	14.38 M Ω
Resistance R_{1dc}	12.2 M Ω

Fig. 17 shows the input/output voltages. Remember that the input voltage is a wave with an amplitude of 279.96 V. The output voltage is lower than the input voltage and has an amplitude of 257.23 V in steady condition. Zoom A makes this point extremely evident.

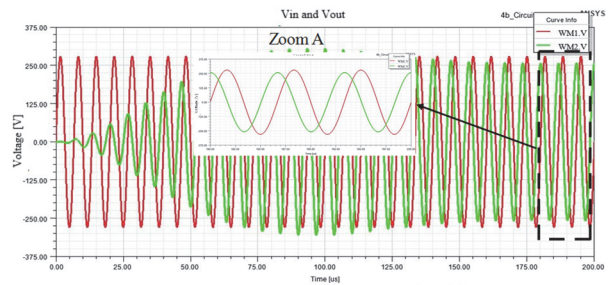


Figure 17 The input and output voltage curves

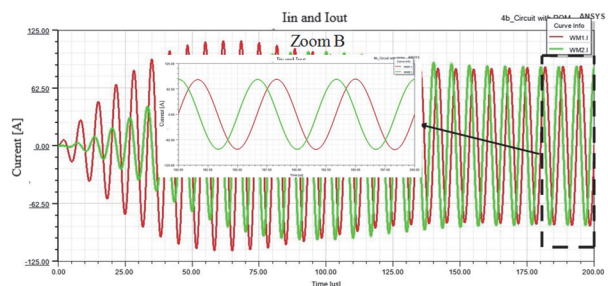


Figure 18 The input and output current curves

Fig. 18 shows the input/output current curves. During a small part of the steady state (Zoom B), the maximum

current values can be read (input current is 85.36A and output current is 85.74A).

Fig. 19 shows that the input and output powers are both present as steady-state waves. The maximum input power is 53.7 KW and the output power lags further than the input power with a maximum value equal to 47.16 KW (max). From the results of the ratio established between the input and output powers, the efficiency is approximately 87.82%.

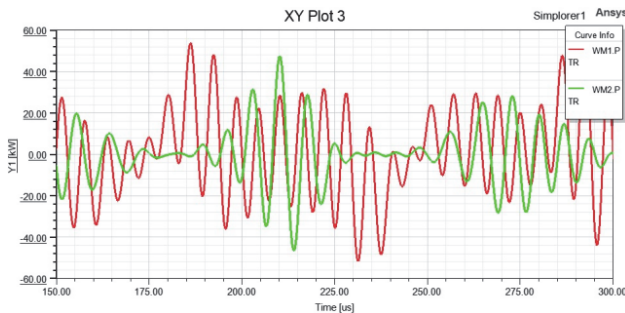


Figure 19 The input and output power curves

According to Fig. 20, the studied highway was supposed to compose a double line. One of them is provided by the wireless recharge system. Each specific number of this transmitter has been supposed to be connected to a PV panels system, noted (L). As static specifications, for each 10 kilometer stretch of highway, 5000 transmitter coils of 120 cm in length are used, with 80 cm between them, as shown in Fig. 20.

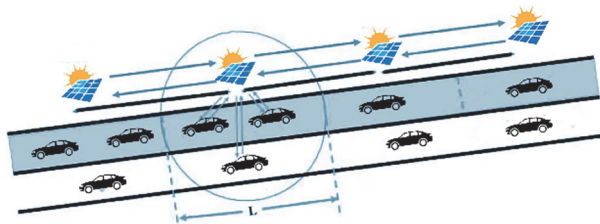


Figure 20 Infrastructure model on the highway

Deploying the wireless charging infrastructure on public highways determines the power transfer and charge density fees. There are two possible system conceptions [40]. 100 KW is the maximum power transfer rate. In the first scenario, let's assume that there is enough electricity for two electric cars on a 50-meter length. An Electric Vehicle is situated every 40 meters in Layout 2, and the maximum power transfer rate is 140 KW. Layout 1 is used in this investigation, and Fig. 21 displays the corresponding model.

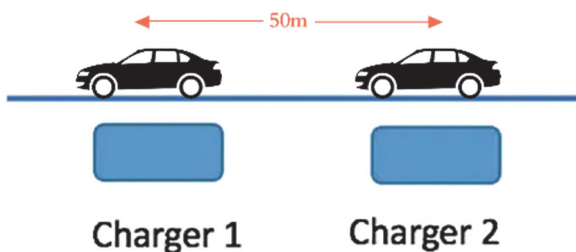


Figure 21 Arrangement on the highway

For this study, each kilometer of a highway has a photovoltaic central plant, so the power will be managed to the transmitter by using an ensemble of switchers on each

coil to make it easier to switch between them while charging the vehicles so that they can be charged conveniently. Fig. 22 effectively illustrates the prototype. The intelligent power management algorithm is not treated in this version. This design cannot be adapted if the different inverters are controlled by a power management tool, which can specify which inverter must be connected in concordance if a vehicle needs charge or not.

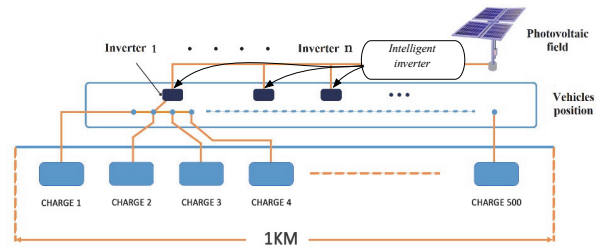


Figure 22 Global architecture for transmitters and PV panels

5 SIMULATION AND RESULTS

The overall system efficiency and performance were evaluated using the Matlab simulation platform. The built model was implemented on an I7 laptop which has 16 Go as Ram.

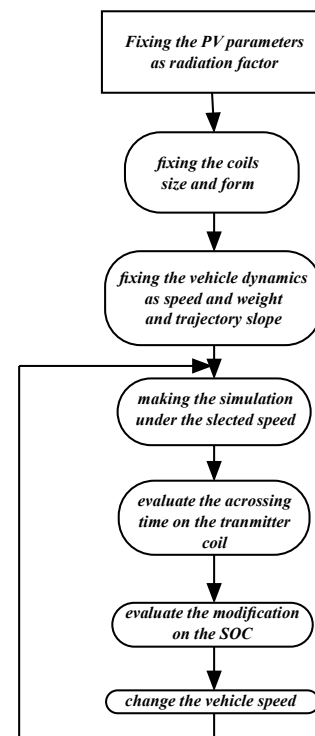


Figure 23 Simulation methodology

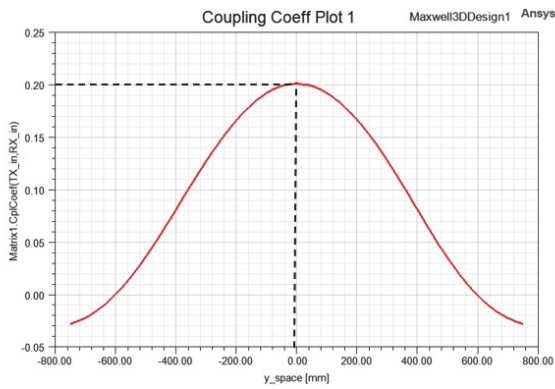
The simulation objective is to have the number of the wireless recharge coil on road that can be used for fully charging a vehicle, if the initial state of charge is 50%. Therefore, the simulation philosophy is to demonstrate, firstly, that the distance between the transmitter and receiver coil can influence the global performances and then, to demonstrate the earned SOC value under the lowest speed and prove that this is dependent on the PV wireless performance as radiation factor and prove the influence of this factor on the overall prototype. As the simulation tests are a lot, the majority of tests were applied

outside of this project and the results were collected in the Tab. 7. The results have been represented for the case of an electric vehicle that will travel one kilometer of a highway equipped with a wireless charger. One kilometer contains 500 transmitters. Tab. 6 exposes the simulation specifications.

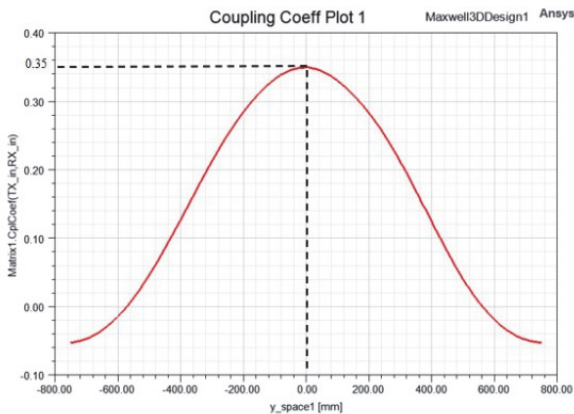
Table 6 Specifications of the simulation phase

Parameter	Value
Number of cars	1
Trajectory distance	1 km
Number of wireless transmitters	500
Coils specification	Tab. 3
Distance between two coils	10 cm
Vehicle speed (km/h)	From 30 to 110
Initial battery state of charge	50%
Simulation Time (Curve 25)	5 seconds

It is mandatory to mention that the distance between the transmitting coils and the receiving coils influences the amount of power transferred. Fig. 24 gives an idea of the effect of distance between transmitter and receiver.



(a)



(b)

Figure 24 Magnetic coupling in the case the centers of the two coils coincide

In Fig. 24a, we notice that the curve of the coupling coefficient increases until it reaches its maximum value at 0.20 for a distance between the two coils equal to 20 cm, In Fig. 24b we observe that the curve of coefficient of coupling increases up to 0.35 for a space between the two coils which is equal to 10 cm. The magnetic coupling will be highest even if the space between the two transmitting and receiving coils is small.

As it is in Tab. 7, for a vehicle speed of 30 km per hour, the 120 cm transmitter coil can recharge the vehicle in a time equal to 0.144 s as shown in Fig. 25. Thus, in a 1 km

segment that contains 500 coils the time to recharge is equal to 120 s. Tab. 7 shows that the EV battery takes less time to recharge as the vehicle speed increases.

The results diagnosis will try to study the vehicle speed's impact on the state of charge for constant climatic conditions, which is supposed to be maximal at the initial test and be varied in the next test case. The battery's initial state of charge is supposed to be 50%, that means when the vehicle is in the region of the wireless recharge section, its battery state of charge is equal to 50%. The vehicle speed was supposed to be constant for all this period, and it is equal to 30km/h. With this speed, the vehicle will cross the recharge region in 120 seconds. That means that the vehicle will be wireless connected to each transmitter for 0.24 seconds. Fig. 25 gives the different dimensions of the overall system which presents the vehicle on the rechargeable road. Based on the given specifications and the mentioned vehicle speed, each coil can be crossed in 0.144 seconds.

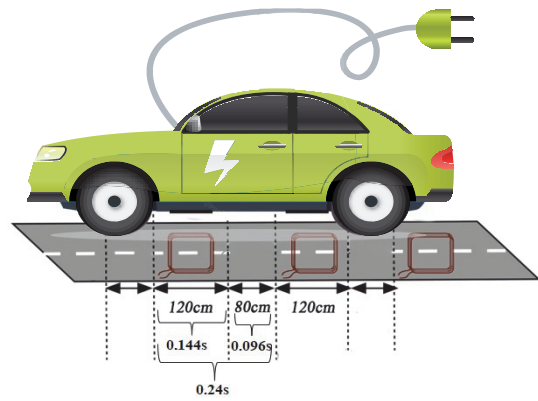


Figure 25 Dimensions of coils on the road and equivalent needed time for crossing the coil by 30 km/h

Based on these specifications and if concentrating on the lowest studied speed (30 km/h), the battery state of charge will change by up to 0.05% in 5 seconds, for the best efficiency factor. Irradiation, and therefore maintaining the same specification on the road and the vehicle, in this case, the battery reaches a value of 51.2% as a new SOC. This case is the best one, as the vehicle needed power is lowest and the recharge time is highest. Fig. 26 shows the Corresponding SOC evolution.

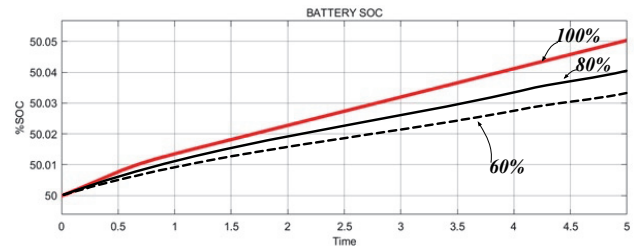


Figure 26 SOC evolution under 30 km/h in 5 seconds as simulation time and for three irradiation factors

The results in Fig. 25, show that solar radiation can influence the system's rentability. This study has a guide to Tab. 7, which can estimate the needed wireless transmitter number for each speed and for having a full recharge if starting from 50%.

Actually, the recharge time was evaluated by passing a single coil receiver above the transmitter by various

speeds, then the connection time was evaluated and the SOC earn was esteemed. For example, for a 30 km/h, the coils will be connected for 0.144 s, which can modify the SOC by 0.0024%. This is equivalent to 1.2 % if 500 coils

are used. After making the calculation model, the number of the esteemed coil for a full recharge under the same speed is 20834 and this can happen in 42 km for the same vehicle speed.

Table 7 Needed KM number of wireless recharge road for full charging an EV which starts by 50% as initial SOC and under 100% as irradiation factor

Vehicle speed / km/h	Recharge time for a single coil	Earn SOC (%) in one KM	Needed Transmitters number for a full charge	Needed Total distance in km
30	0.144 s	1.2	20834	42
60	0.072 s	0.72	34723	70
70	0.0514 s	0.65	38462	78
90	0.04 s	0.42	59524	120
100	0.036 s	0.38	65790	132
110	0.0327 s	0.32	78125	157

Based on the obtained results, the following four points can be used to list the outcomes:

The PV radiation factor has a major influence on the status of the charge, and greater radiation factors are associated with favorable situations. It has been shown that vehicle speed significantly affected the overall effectiveness of the recharge tool, with the lowest selected speed exhibiting the greatest results. Moreover, we have determined that the maximum vehicle speed at which the transmitter coil count must be selected may complicate the road trajectory as a whole.

6 FUTURE ENDEAVORS AND HOW THIS RESEARCH SOLVES THE SAFETY FACTOR

This study explores the use of renewable energy sources, such as PV generators, in wireless charging systems, demonstrating the potential advantages of reducing dependence on the electrical grid and ensuring the uninterrupted charging of electric vehicles. Furthermore, by examining how different conditions, such as vehicle speed and climate, affect the wireless charging system's performance, this study can also help optimize its efficiency and address safety concerns. Overall, the study provides a framework for developing and deploying more sustainable and efficient PV-wireless charging systems for electric vehicles on highways.

Conversely, an important question can be asked about how the research solves the safety issues raised by using PV-wireless charging systems on highways. This can be resolved by using photovoltaic (PV) generators as an alternative source for wireless charging systems, which may alleviate safety concerns. Using solar energy to generate electricity reduces carbon emissions and promotes sustainability by using renewable energy sources. In addition to examining how various vehicle conditions affect wireless charging, such as speed and climate, the researchers also evaluate how the system can be made safer and more efficient.

7 CONCLUSIONS

This work designs and studies detailed research of dynamic wireless power transmission for a highway application. The current condition of the system was explained, along with how it relates to EV applications. To perform correctly the system examination, the mathematical bloc of each part in this recharge system was described and discussed. Matlab Simulink and ANSYS

Maxwell were used as simulation tools for completely testing the efficiency of the recharge system under various speeds and by using a renewable energy source based on solar radiation. The results prove that even if the vehicle speed is high, it will be necessary to have a larger number of coil transmitters and then more distance on the road must be equipped with that transmitter. The study has been conducted to have 157 km equipped with more than 78000 transmitters for having a full battery recharge if starting by 50% as battery SOC.

Also, this study has demonstrated that several factors can react to the global system, and it is not easy to estimate the necessary number of transmitters if the climate factor changes or if the vehicle-driven mode is different from the standard norms. As a result, one of the work's future goals is to test more than only drive cycle mode and investigate the impact of vehicle weight change on the road on battery performance.

Acknowledgements

The authors extend their appreciation to the Deanship of Scientific Research at Northern Border University, Arar, KSA for funding this research work through the project number NBU-FFR-2023-0167. The authors gratefully thank the Prince Faisal bin Khalid bin Sultan Research Chair in Renewable Energy Studies and Applications (PFCRE) at Northern Border University for their support and assistance.

8 REFERENCES

- [1] Arif, S. M., Lie, T. T., Seet, B. C., Ayyadi, S., & Jensen, K. (2021). Review of electric vehicle technologies, charging methods, standards and optimization techniques. *Electronics*, 10(16), 1910. <https://doi.org/10.3390/electronics10161910>
- [2] Mahesh, A., Chokkalingam, B., & Mihet-Popa, L. (2021). Inductive wireless power transfer charging for electric vehicles--a review. *IEEE Access*, 9, 137667-137713. <https://doi.org/10.1109/ACCESS.2021.3116678>
- [3] Giannakis, E., Serghides, D., Dimitriou, S., & Zittis, G. (2020). Land transport CO₂ emissions and climate change: evidence from Cyprus. *International Journal of Sustainable Energy*, 39(7), 634-647. <https://doi.org/10.1080/14786451.2020.1743704>
- [4] Stamati, T.-E. & Bauer, P. (2012). Green energy for on-road charging of electric vehicles. *Proceedings of 15th international conference Mechatronika*, 1-9.
- [5] Jiang, A., Maglaras, F. V., & Moschoyiannis, S. (2015). Dynamic wireless charging of electric vehicles on the move

- with Mobile Energy Disseminators. *International Journal of Advanced Computer Science and Applications*, 6(6). <https://doi.org/10.14569/IJACSA.2015.060634>
- [6] Lu, C., Zhou, H., Li, L., Yang, A., Xu, C., Ou, Z., & Tian, F. (2022). Split-core magnetoelectric current sensor and wireless current measurement application. *Measurement: journal of the International Measurement Confederation*, 188, 110527. <https://doi.org/10.1016/j.measurement.2021.110527>
- [7] Liu, G. (2021). Data Collection in MI-Assisted Wireless Powered Underground Sensor Networks: Directions, Recent Advances, and Challenges. *IEEE Communications Magazine*, 59(4), 32-138. <https://doi.org/10.1109/MCOM.001.2000921>
- [8] Wu, H., Jin, S., & Yue, W. (2022). Pricing Policy for a Dynamic Spectrum Allocation Scheme with Batch Requests and Impatient Packets in Cognitive Radio Networks. *Journal of Systems Science and Systems Engineering*, 31(2), 133-149. <https://doi.org/10.1007/s11518-022-5521-0>
- [9] Liu, X., Li, Z., Fu, X., Yin, Z., Liu, M., Yin, L., & Zheng, W. (2023). Monitoring House Vacancy Dynamics in The Pearl River Delta Region: A Method Based on NPP-VIIRS Night-Time Light Remote Sensing Images. *Land*, 12(4). <https://doi.org/10.3390/land12040831>
- [10] Luo, Z., Cai, S., Hao, S., Bailey, T. P., Luo, Y., Luo, W., & Kanatzidis, M. G. (2021). Extraordinary role of Zn in enhancing thermoelectric performance of Ga-doped n-type PbTe. *Energy and Environment Science*, 15. <https://doi.org/10.1039/d1ee02986j>
- [11] Song, J., Mingotti, A., Zhang, J., Peretto, L., & Wen, H. (2022). Accurate Damping Factor and Frequency Estimation for Damped Real-Valued Sinusoidal Signals. *IEEE Transactions on Instrumentation and Measurement*, 71. <https://doi.org/10.1109/TIM.2022.3220300>
- [12] Lu, L., Wu, W., Gao, Y., Pan, C., Yu, X., Zhang, C., & Jin, Z. (2022). Study on current discrepancy and redistribution of HTS non-insulation closed-loop coils during charging/discharging and subsequent transient process toward steady-state operation. *Superconductor Science and Technology*, 35(9), 95001. <https://doi.org/10.1088/1361-6668/ac7dfe>
- [13] Zhang, X., Wang, Y., Yuan, X., Shen, Y., Lu, Z., & Wang, Z. (2022). Adaptive Dynamic Surface Control with Disturbance Observers for Battery/Supercapacitor-based Hybrid Energy Sources in Electric Vehicles. *IEEE Transactions on Transportation Electrification*. <https://doi.org/10.1109/TTE.2022.3194034>
- [14] Zhang, X., Lu, Z., Yuan, X., Wang, Y., & Shen, X. (2021). L2-Gain Adaptive Robust Control for Hybrid Energy Storage System in Electric Vehicles. *IEEE Transactions on Power Electronics*, 36(6), 7319-7332. <https://doi.org/10.1109/TPEL.2020.3041653>
- [15] Wu, Z., Lin, B., Fan, J., Zhao, J., Zhang, Q., & Li, L. (2022). Effect of Dielectric Relaxation of Epoxy Resin on Dielectric Loss of Medium-Frequency Transformer. *IEEE Transactions on Dielectrics and Electrical Insulation*, 29(5), 1651-1658. <https://doi.org/10.1109/TDEI.2022.3193652>
- [16] Zheng, X., Cai, G., Guo, J., Gao, W., Huang, Y., & Tong, X. (2023). Combustion characteristics and thermal decomposition mechanism of the flame-retardant cable in urban utility tunnel. *Case Studies in Thermal Engineering*, 44, 102887. <https://doi.org/10.1016/j.csite.2023.102887>
- [17] Liu, Z., Li, H., Hou, K., Xu, X., Jia, H., Zhu, L., & Mu, Y. (2023). Risk assessment and alleviation of regional integrated energy system considering cross-system failures. *Applied Energy*, 350, 121714. <https://doi.org/10.1016/j.apenergy.2023.121714>
- [18] Ma, X., Liao, Z., Wang, Y., & Zhao, J. (2023). Fast Dynamic Phasor Estimation Algorithm Considering DC Offset for PMU Applications. *IEEE Transactions on Power Delivery*. <https://doi.org/10.1109/TPWRD.2023.3285949>
- [19] Yuan, C., Liu, D., Zhu, Y., Zeng, T., Jiang, B., Tang, C., & Li, Q. (2023). Effect of charge transport on electrical degradation in polypropylene/organic molecular semiconductor composites for HVDC cable insulation. *Applied Physics Letters*, 122(11). <https://doi.org/10.1063/5.0133417>
- [20] Li, X., Aftab, S., Abbas, A., Hussain, S., Aslam, M., Kabir, F., & Ansari, M. Z. (2023). Advances in mixed 2D and 3D perovskite heterostructure solar cells: A comprehensive review. *Nano Energy*, 118, 108979. <https://doi.org/10.1016/j.nanoen.2023.108979>
- [21] Shen, Y., Xie, J., He, T., Yao, L., & Xiao, Y. (2023). CEEMD-fuzzy Control Energy Management of Hybrid Energy Storage Systems in Electric Vehicles. *IEEE Transactions on Energy Conversion*. <https://doi.org/10.1109/TEC.2023.3306804>
- [22] Qiu, Y., Shi, M., Guo, X., Li, J., Wu, J., Zhou, Y., & Li, Y. (2023). Sensitivity improvement in the measurement of minor components by spatial confinement in fiber-optic laser-induced breakdown spectroscopy. *Spectrochimica Acta Part B: Atomic Spectroscopy*, 209, 106800. <https://doi.org/10.1016/j.sab.2023.106800>
- [23] Shirkhani, M., Tavoosi, J., Danyali, S., Sarvenoe, A. K., Abdali, A., Mohammadzadeh, A., & Zhang, C. (2023). A review on microgrid decentralized energy/voltage control structures and methods. *Energy Reports*, 10, 368-380. <https://doi.org/10.1016/j.egy.2023.06.022>
- [24] Lin, L., Zhang, J., Gao, X., Shi, J., Chen, C., & Huang, N. (2023). Power fingerprint identification based on the improved VI trajectory with color encoding and transferred CBAMResNet. *PLoS one*, 18(2), e0281482. <https://doi.org/10.1371/journal.pone.0281482>
- [25] Wang, H., Wang, B., Luo, P., Ma, F., Zhou, Y., & Mohamed, M. A. (2022). State Evaluation Based on Feature Identification of Measurement Data: for Resilient Power System. *CSEE Journal of Power and Energy Systems*, 8(4), 983-992. <https://doi.org/10.17775/CSEEJPES.2021.01270>
- [26] Luo, P., Wang, B., Wang, H., Ma, F., Ma, H., & Wang, L. (2023). An Ultrasmall Bolt Defect Detection Method for Transmission Line Inspection. *IEEE Transactions on Instrumentation and Measurement*, 72. <https://doi.org/10.1109/TIM.2023.3241994>
- [27] Li, P., Hu, J., Qiu, L., Zhao, Y., & Ghosh, B. K. (2022). A Distributed Economic Dispatch Strategy for Power - Water Networks. *IEEE Transactions on Control of Network Systems*, 9(1), 356-366. <https://doi.org/10.1109/TCNS.2021.3104103>
- [28] Duan, Y., Zhao, Y., & Hu, J. (2023). An initialization-free distributed algorithm for dynamic economic dispatch problems in microgrid: Modeling, optimization and analysis. *Sustainable Energy, Grids and Networks*, 34, 101004. <https://doi.org/10.1016/j.segan.2023.101004>
- [29] Zhou, S., Zhou, G., Liu, X., & Zhao, H. (2023). Dynamic Freewheeling Control for SIDO Buck Converter With Fast Transient Performance, Minimized Cross-Regulation, and High Efficiency. *IEEE Transactions on Industrial Electronics*, 70(2), 1467-1477. <https://doi.org/10.1109/TIE.2022.3156169>
- [30] Zhou, S., Zhou, G., He, M., Mao, S., Zhao, H., & Liu, G. (2023). Stability Effect of Different Modulation Parameters in Voltage-Mode PWM Control for CCM Switching DC-DC Converter. *IEEE Transactions on Transportation Electrification*. <https://doi.org/10.1109/TTE.2023.3293811>
- [31] Chen, H., Wu, H., Kan, T., Zhang, J., & Li, H. (2023). Low-carbon economic dispatch of integrated energy system containing electric hydrogen production based on VMD-GRU short-term wind power prediction. *International Journal of Electrical Power & Energy Systems*, 154, 109420. <https://doi.org/10.1016/j.ijepes.2023.109420>

- [32] Zhang, L., Yin, Q., Zhu, W., Lyu, L., Jiang, L., Koh, L. H., & Cai, G. (2023). Research on the orderly charging and discharging mechanism of electric vehicles considering travel characteristics and carbon quota. *IEEE Transactions on Transportation Electrification*.
https://doi.org/10.1109/TTE.2023.3296964
- [33] Xiao, S., Wang, Z., Wu, G., Guo, Y., Gao, G., Zhang, X., & Li, P. (2023). The impact analysis of operational overvoltage on traction transformers for high-speed trains based on the improved capacitor network methodology. *IEEE Transactions on Transportation Electrification*.
https://doi.org/10.1109/TTE.2023.3283668
- [34] Wang, Z., Li, J., Hu, C., Li, X., & Zhu, Y. (2024). Hybrid energy storage system and management strategy for motor drive with high torque overload. *Journal of Energy Storage*, 75, 109432. https://doi.org/10.1016/j.est.2023.109432
- [35] Jasim, A. M., Jasim, B. H., Alhasnawi, B. N., Flah, A., & Kraiem, H. (2023). Coordinated Control and Load Shifting-Based Demand Management of a Smart Microgrid Adopting Energy Internet. *International Transactions on Electrical Energy Systems*, 2023, 6615150.
https://doi.org/10.1155/2023/6615150
- [36] Guingane, T. T., Koalaga, Z., Simonguy, E., Zougmore, F., & Bonkougou, D. (2016). Modélisation et simulation d'un champ photovoltaïque utilisant un convertisseur élévateur de tension (boost) avec le logiciel MATLAB/SIMULINK. *Journal International de Technologie, de l'Innovation, de la Physique, de l'Energie et de l'Environnement*, 2(1).
- [37] Hananou, F. & Rouabah, A. (2014). Modélisation et simulation d'un système photovoltaïque.
- [38] Kraiem, H., Aymen, F., Yahya, L., Triviño, A., Alharthi, M., & Ghoneim, S. S. M. (2021). A Comparison between Particle Swarm and Grey Wolf Optimization Algorithms for Improving the Battery Autonomy in a Photovoltaic System. *Applied Sciences*, 11(16), 1-19.
https://doi.org/10.3390/app11167732
- [39] Inoue, S., Nimri, R., Kamineni, A., & Zane, R. (2021). A New Design Optimization Method for Dynamic Inductive Power Transfer Systems utilizing a Neural Network. *2021 IEEE Energy Conversion Congress and Exposition (ECCE)*, 1496-1501. https://doi.org/10.1109/ECCE47101.2021.9595560

Contact information:**Asma BOUKHCHANA**

University of Gabès, Gabès 6072, Tunisia
E-mail: asma.boukchana@gmail.com

Mohamed NAoui

University of Gabès, Gabès 6072, Tunisia
E-mail: mohamednaoui60@gmail.com

Aymen FLAH

- 1) Energy Processes Environment and Electrical Systems Unit, National Engineering School of Gabès, University of Gabès, Gabès, 6029, Tunisia
- 2) University of Business and Technology (UBT), College of Engineering, Jeddah, 21448, Saudi Arabia
- 3) MEU Research Unit, Middle East University, Amman, 11831, Jordan
- 4) University of Gabès, Private Higher School of Applied Sciences and Technology of Gabès, Gabès, 6029, Tunisia
- 5) Applied Science Research Center, Applied Science Private University, Amman, 11931, Jordan

Habib KRAIEM

(Corresponding author)
Department of Electrical Engineering,
College of Engineering, Northern Border University,
Arar, Saudi Arabia
E-mail: alhabeeb.kareem@nbu.edu.sa